AIAA 81-4261

Potential Flow about Bodies of Revolution with Mixed Boundary Conditions—Axial Flow

J.V. Rattayya,* J.A. Brosseau,† and M.A. Chisholm‡
Lockheed Missiles & Space Company, Inc., Sunnyvale, Calif.

The potential flow past an axisymmetric body in the presence of a gravitational field with mixed boundary conditions has been solved using an iterative technique, and assigning sources on the body-cavity surface. To avoid the computational difficulties associated with the cavity closure conditions, a constant-pressure boundary condition has been imposed only on the portion of the cavity close to the body base. The pressure distributions and cavity configuration so computed in the vicinity of the body base are compared at different Froude numbers and base-pressure coefficients with measurements made in wind tunnel and in underwater free-flight conditions. The agreement reasonably justifies the computational method. For the case of a 5 deg cone, the present method is also compared with existing analytical solutions based on the axial distribution of singularities and the slender body assumption.

Nomenclature

C_p = pressure coefficient, Eq. (10)
d = body base diameter
F = Froude number, Eq. (10)
g = gravitational acceleration
L_B = body length
L_C = cavity length
p = pressure
p_∞ = freestream pressure
$R_B(x)$ = body radius
$R_c(x)$ = cavity radius
r = radial distance from axis of asymmetry
r_{pQ} = linear distance between points p and Q
S = distance along meridian
s = surface area
U_∞ = freestream velocity
V_N = velocity in direction normal to the body
V_S = velocity along the meridian line
x,y,z = rectangular coordinate system
Φ = velocity potential
ϕ = perturbation velocity potential
ρ = fluid density
θ = circumferential angle
β = body slope
$\delta(x)$ = Dirac delta function

Subscripts

B = body
b = base
c = cavity

I. Introduction

THE hydrodynamic flow past a blunt-based body of revolution is plagued at high speeds with the formation of a cavity behind the body. This region is separated from the main potential flow by means of a thin shear layer or a free-stream surface. For purposes of analysis, the pressure in this region can be treated as remaining constant. Experimental evidence suggests that the size of the cavity is dependent on the pressure inside the cavity, and the body axial velocity. Thus, to be more exact, the analysis of the potential flowfield about a blunt-based body requires the satisfaction of a constant pressure condition on the cavity surface, which is different from that of a rigid surface boundary condition ahead of it. This paper is directed at solving the potential flowfield around bodies of revolution with such mixed boundary conditions and in the presence of a gravity field.

The analyses of potential flows past bodies of revolution have been made earlier,[1-5] but with restrictive assumptions. Cuthbert and Street,[1] and Chou[2] both assumed that the body was slender and distributed singularities (sources and sinks) on the body-cavity axis for the potential flow solution, but differed in their treatment of the cavity-closure. Specifically, a modified Riabouchinsky model was employed in Ref. 1 to close the cavity, while a rear stagnation point was assumed in Ref. 2 at the point of closure. Mathematically, both models reduced to similar nonlinear integral differential equations, which were then solved to determine the cavity shape and the resultant flowfield. The influence of a vertical gravity field acting along the body axis was included in both of these analyses. However, the applicability of these models is restricted, depending on the slenderness of the body-cavity system, to low cavitation and high Froude numbers. In actual applications, flows of much higher cavitation and lower Froude numbers are of interest.

The assumption of slenderness was removed, and the exact potential flow solutions for bodies of revolution were constructed in Refs. 3 and 4 by distributing the sources on the body surface instead of on the body axis. Struck[3] treats the mixed-boundary value problem and calculated the cavity surface by an iteration technique. Smith and Pierce,[4] on the other hand, consider strictly a rigid body with flow fully attached to it. Both of these papers ignore the gravity field entirely.

In flows past underwater bodies with smooth contours, the flow is attached over the body surface and it separates only at the base to form a cavity. In this paper, the exact solution for potential flow past an axisymmetric body with such a prescribed flow separation boundary is developed, taking gravity into account. Thus, this forms essentially an extension of Struck's work reported in Ref. 3, and is particularly applicable to compute flowfields and cavity configurations associated with vertically launched underwater missiles. Due to the lack of information on specific cavity configurations, and/or analytical methods to account for their effects on missiles, past analyses (see for example Ref. 5) assume a straight cylindrical extension of the missile to simulate a trailing

Received Aug. 1, 1979; revision received Aug. 22, 1980.

*Staff Engineer. Member AIAA.
†Research Specialist.
‡Research Specialist.

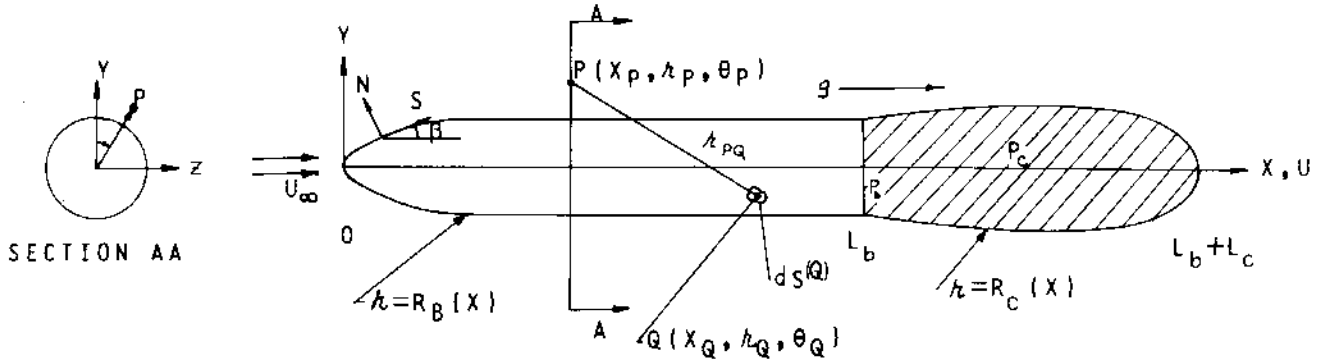

Fig. 1 Body-cavity configuration.

cavity. Such an assumption would naturally lead to somewhat erroneous hydrodynamic loading on the missile than would occur in the presence of an actual trailing cavity. Potential flow analysis with mixed boundary conditions, and the iterative technique developed to compute the cavity shape is presented and discussed in Sec. II. Typical numerical results are computed in Sec. III, and then compared with wind tunnel data and free-flight test data of models launched vertically under water. Additional comparisons with earlier analysis (Ref. 5) are also made in this section.

II. Analytical Problem and its Method of Solution

Governing Equations

Consider an axisymmetric body of radius $R_B(x)$ and length L_B travelling with velocity U_∞ along its axis of symmetry in an ideal fluid of density ρ. Let us assume an axisymmetric cavity of finite length and radius $R_c(x)$ has been trailing attached to this body as shown in Fig. 1. The cavity configuration depends on the body velocity U_∞ and the base pressure, p_b, and is unknown. Since the body-cavity configuration is axisymmetric, it is convenient to choose a cylindrical coordinate system (x, r, θ) with its origin located at the nose of the body and x-axis, along its symmetric axis positive toward the base. In this body-fixed coordinate system, the flow appears to be coming from the left and the velocity potential Φ can be written as

$$\Phi(x,r) = U_\infty [x+\phi(x,r)] \tag{1}$$

where the first term represents the onset flow, and the second term the perturbation velocity potential. The perturbation potential that satisfies $\nabla^2\phi=0$ in the fluid medium along with the radiation condition $\phi\to 0$ at infinity can be expressed in the form of a surface integral. The potential ϕ_P at field point P is

$$\phi_P(x_P,r_P) = \iint_{S_B+S_c} \frac{\sigma^{(Q)}\,ds^{(Q)}}{r_{PQ}} \tag{2}$$

Here $\sigma^{(Q)}$ represents the source strength distribution at the point Q on the body or cavity surface; $ds^{(Q)}$ an elemental surface area surrounding Q; and r_{PQ} the linear distance between the points P and Q.

$$r_{PQ} = (x_P-x_Q)^2 + (y_P-y_Q)^2 + (z_P-z_Q)^2$$

where

$$\begin{aligned} y_P &= r_P\cos\theta_P \qquad & z_P &= r_P\sin\theta_P \\ y_Q &= r_Q\cos\theta_Q \qquad & z_Q &= r_Q\sin\theta_Q \end{aligned} \tag{3}$$

Note the integration in Eq. (2) extends over the whole body-cavity surface, s_B+s_c. Because the flow is symmetric about the x-axis, the source strength σ_Q does not vary circumferentially. Though the integrand in Eq. (2) depends on the circumferential angles θ_P and θ_Q, the surface integration cancels the θ-dependence and the velocity potential becomes independent of θ.

The requirement of zero flow normal to the rigid body surface, as well as the trailing cavity, reduces to the condition

$$\frac{\partial\Phi}{\partial N} = 0 \qquad \text{on} \qquad s_B, s_c \tag{4}$$

where N indicates the unit distance normal to the body-cavity surface. If the gravity field g acts along the x-axis, the Bernoulli equation along the stream line forming the body-cavity system yields

$$p_\infty + \tfrac{1}{2}\rho U_\infty^2 = p + \tfrac{1}{2}\rho(\partial\Phi/\partial S)^2 - \rho g(x-L_B) \tag{5}$$

where, for convenience, the gravity level is referenced at the base of the body. Note $\partial\Phi/\partial S$ represents the flow velocity along the stream line relative to the body. If the cavity is assumed quiescent inside, the pressure p in Eq. (5) must equal the pressure p_c inside the cavity. Furthermore, the pressure p_c is uniform and equals the base pressure p_b. Thus, the additional condition appropriate at the cavity-fluid interface becomes

$$p_b - p_\infty = \tfrac{1}{2}\rho[U_\infty^2 - (\partial\Phi/\partial S)^2] + \rho g(x-L_B) \tag{6}$$

Note the velocity potential Φ depends on the cavity configuration $R_c(x)$, which is still unknown. The basic mathematical problem, therefore, is to find $\sigma_{(Q)}$ and $R_c(x)$ such that Eqs. (4) and (6) are simultaneously satisfied.

To construct the solution, one chooses the field point P on the surface of the body itself. The boundary condition, Eq. (4), at point P is expressed in the form[4]

$$\begin{aligned} &-2\pi\sigma^{(P)} - \sin\beta^{(P)} \iint_{S_B+S_c} \sigma^{(Q)} \frac{\partial}{\partial x}\left(\frac{1}{r_{PQ}}\right) ds^{(Q)} \\ &+ \cos\beta^{(P)} \iint_{S_B+S_c} \sigma^{(Q)} \frac{\partial}{\partial y}\left(\frac{1}{r_{PQ}}\right) ds^{(Q)} \\ &- \sin\beta^{(P)} = 0 \qquad \text{on} \qquad s_B, s_c \end{aligned} \tag{7}$$

where β is dependent on the body geometry, and is related to the body slope through the relation

$$dR/dx = \tan\beta \tag{8}$$

The pressure condition, Eq. (6), is first rewritten in the nondimensional form

$$C_{p_b} = 1 - \left[\frac{1}{U_\infty}\frac{\partial\Phi^{(P)}}{\partial S}\right]^2 + 2(x-L_B)L_B^{-1}F^{-2} \tag{9}$$

where the familiar definitions of pressure coefficient C_p and Froude number F are used:

$$C_p = (p - p_\infty) / \tfrac{1}{2}\rho U_\infty^2 \qquad F^2 = U_\infty^2 / gL_B \tag{10}$$

Solving this equation for $\left[\frac{1}{U_\infty}\frac{\partial\Phi}{\partial S}\right]^{(P)}$ on the cavity one has

$$\left[\frac{1}{U_\infty}\frac{\partial\Phi}{\partial S}\right]^{(P)} = V_S^{(P)} = \sqrt{1 - C_{p_b} + 2(x - L_B)L_B^{-1}F^{-2}} \qquad (x \geq L_B) \tag{11}$$

Note the right-hand side of this equation is real and positive for all $x > L_B$ and $C_{p_b} \leq 1.0$. Also, for a given value of base pressure coefficient, C_{p_b}, this increases with distance downstream from the base. Substituting for Φ, this constant pressure condition can be expressed as the integral differential equation for the cavity part of the problem:

$$\cos\beta^{(P)}\left[1 + \iint_{S_B+S_c} \sigma^{(Q)}\frac{\partial}{\partial x}\left(\frac{1}{r_{PQ}}\right)dS^{(Q)}\right] + \sin\beta^{(P)}\iint_{S_B+S_c}\sigma^{(Q)}\frac{\partial}{\partial y}\left(\frac{1}{r_{PQ}}\right)dS^{(Q)} = V_S^{(P)} \tag{12}$$

The mathematical problem posed here thus reduces to solving the integral differential Eq. (7) for source strength $\sigma(x)$, such that the pressure condition Eq. (12) is satisfied on the cavity surface, $R_c(x)$, which also needs to be evaluated as a part of the solution.

Method of Solution

The numerical solution to the problem with no flow separation and formation of the trailing cavity is somewhat straightforward, and has been thoroughly discussed in Ref. 4. In this case, the problem reduces to satisfying Eq. (7) only, and can be solved to any degree of accuracy with the high-speed computer. The basic approach taken is to divide the body of revolution into a finite number, say N, of conical segments and impose the condition, Eq. (7), at the center of each segment along one meridian line, $\theta = 0$. Such a scheme leads to N coupled, linear, nonhomogeneous algebraic equations for N unknown values of σ at the center of each conical segment. In Ref. 4, for simplicity, the source strength σ is assumed constant on each conical segment. This assumption has been relaxed, and is replaced with the linear variation of σ over each segment in Ref. 6. This modification has improved the numerical accuracy of the solution considerably, and is used in the calculations reported in this paper. The equations are then solved for N values of σ, and the function $\sigma(x)$ so calculated is substituted in the discrete version of Eq. (2) to calculate the potential function anywhere in the flowfield.

The direct extension of this technique to the problem of a trailing cavity becomes difficult for two reasons. First, the cavity radius $R_c(x)$ and hence $\beta_c(x)$ is not known a priori, and needs to be computed as part of the solution. Second, in addition to the zero normal velocity boundary condition, Eq. (7), the constant pressure condition, Eq. (12), has also to be satisfied simultaneously. The numerical technique thus results in more equations than the unknowns and, hence, the exact solution is not possible in a single step. For this reason, an iteration technique has been developed wherein the basic technique is still retained and used repeatedly, while the additional boundary conditions are used to update the cavity radius prior to each succeeding iteration. To be more specific, in each iteration the boundary condition, Eq. (7), is imposed on the rigid body and pressure condition, Eq. (12), on the cavity surface. The resulting solution, then, suggests that the assumed cavity boundary is not a streamline, implying that Eq. (7) is violated over that surface. The boundary is then adjusted to coincide with the computed velocity vector along the cavity. This new boundary is more likely to be a streamline, hence Eq. (7) is more likely to be satisfied along it. These calculations are repeated until no more adjustment to the cavity boundary is needed.

Experience has indicated that the solution converges slowly if the direct satisfaction of Eq. (12) is imposed on the cavity surface. To accelerate the convergence, it is found desirable, in addition, to impose on the cavity surface the velocity potential appropriate to this velocity distribution as well. The basic equations that lead to this final iterative procedure are discussed next.

To start, let us assume a cavity shape $R_c'(x)$. Let $\phi'(x)$ and $V_S'(x)$ be the perturbation velocity potential and the corresponding tangential velocity on the body-cavity system. These quantities are related to each other on the cavity through the relation

$$\phi'(x) = \phi'(L_B) + \int_{L_B}^{x} V_S'(x)\sec\beta'(x)\,dx \qquad (L_B \leq x \leq L_B + L_c) \tag{13}$$

If $\phi(x)$ and $V_S(x)$ are the exact values on the actual body-cavity system one has a relation similar to Eq. (13)

$$\phi(x) = \phi(L_B) + \int_{L_B}^{x} V_S(x)\sec\beta(x)\,dx \quad (L_B \leq x \leq L_B + L_c) \tag{14}$$

Adding and subtracting $\phi'(x)$ to this relation, one writes

$$\phi(x) = \bar{\phi}(x) + \delta\phi(x) \tag{15}$$

where

$$\bar{\phi}(x) = \phi'(x) + \int_{L_B}^{x}(V_S - V_S')\sec\beta'\,dx$$

$$\delta\phi(x) = \phi(L_B) - \phi'(L_B) + \int_{L_B}^{x} V_S(\sec\beta - \sec\beta')dx \qquad (L_B \leq x \leq L_B + L_c) \tag{16}$$

Note, for assumed cavity shape, $\phi'(x)$ and $V_S'(x)$ can be computed. The tangential velocity distribution, $V_S(x)$, is prescribed on the cavity surface, and is equal to the right-hand side of Eq. (11). Thus, the first term $\bar{\phi}(x)$ is a known quantity. Since $\phi(L_B)$ and the slope β of the actual cavity are not known, $\delta\phi(x)$ is an unknown function. Note, as the approximate cavity surface approaches the real cavity configuration, the quantities β', $\phi'(L_B)$, V_S' approach β, $\phi(L_B)$, and V_S, respectively, everywhere on the cavity. This makes $\delta\phi(x)$ tend to zero, while $\phi'(x)$ and $\bar{\phi}(x)$ approach $\phi(x)$. Thus, for cavity shapes that are very close to the actual one, $\delta\phi(x)$ is relatively small, and $\bar{\phi}(x)$ serves as a good guess for the velocity potential on the actual cavity. Let $\bar{V}_S(x)$ be the velocity distribution along the assumed cavity surface corresponding to this potential $\bar{\phi}(x)$. This velocity distribution is expected to be very close to, but not identical with, the desired velocity distribution given on the right-hand side of Eq. (11). The unknown distribution $\delta\phi(x)$ should be such as to account for this difference in velocity distribution.

To develop the iteration technique, one solves the boundary value problem with zero normal velocity, Eq. (7), on the body, and prescribed velocity potential $\bar{\phi}(x)$ on the assumed cavity. Such a solution is straightforward, and can be computed exactly. Let $\bar{\sigma}(x)$ and $\bar{V}_S(x)$ be such solutions for the source strength and tangential velocity distributions. Simi-

larly, one can solve the boundary value problem, satisfying Eq. (7) on the body, and $\phi(x)=\delta(x-x^*)$ on the cavity, without any difficulty. If $\sigma(x;\, x^*)$ and $V_S(x;\, x^*)$ are the source strength and velocity distributions so computed, one could obtain the net source strength $\sigma(x)$ and velocity distribution $V_S(x)$ corresponding to the satisfaction of Eq. (7) on the body, and Eq. (15) on the cavity by simple superposition. They are

$$\sigma(x)=\bar{\sigma}(x)+\int_{L_B}^{L_B+L_c}\sigma(x;\, x^*)\,\delta\phi(x^*)\,dx^* \tag{17a}$$

$$V_S(x)=\bar{V}_S(x)+\int_{L_B}^{L_B+L_c}V_S(x;\, x^*)\,\delta\phi(x^*)\,dx^* \tag{17b}$$

Equating this velocity distribution to the right-hand side of Eq. (11) one obtains

$$\int_{L_B}^{L_B+L_c}V_S(x;\, x^*)\,\delta\phi(x^*)\,dx^*$$

$$=[1-C_{p_b}+2(x-L_B)F^{-2}L_B^{-1}]^{1/2}-\bar{V}_S(x)$$

$$(L_B\le x\le L_B+L_c) \tag{18}$$

In this relation, every quantity is known except $\delta\phi(x^*)$. By converting this integral equation into a matrix equation, one can obtain, numerically, values of $\delta\phi$ at a finite number of points on the cavity surface. The use of this solution in Eq. (17a) determines the desired source strength $\sigma(x)$. Having known $\sigma(x)$, one can compute the normal velocity V_N on the cavity surface. Since the assumed cavity boundary is not correct, the normal velocity V_N is nonzero. The fact that V_N must be zero on the cavity, can be used to compute the new cavity configuration. Knowing $dx'/dS\,(=\cos\beta')$ and $dR_c'/dS\,(=\sin\beta')$ on the assumed cavity configuration, those corresponding to the new configuration can be computed from

$$\frac{dx}{dS}=\frac{dx'}{dS}-\frac{dR'}{dS}\,\frac{V_N(S)}{V_S(S)}$$

$$\frac{dR}{dS}=\frac{dR'}{dS}+\frac{dx'}{dS}\,\frac{V_N(S)}{V_S(S)}$$

The slope β along the new configuration becomes

$$\frac{dR}{dx}=\tan\beta=\frac{dR}{dS}\Big/\frac{dx}{dS}$$

After solving for the new cavity configuration, the values of $\phi'(x)$, $V_S'(x)$ and hence $\bar{\phi}(x)$ are computed again, and the rest of the calculations are repeated until the cavity shape is updated.

This process is repeated until the cavity boundary does not change significantly and $\delta\phi$ assumes almost zero values on the cavity surface.

Cavity Closure

As long as the fluid-cavity interface is assumed a streamline, and the cavity is quiescent inside, the only boundary condition to be satisfied is the constant pressure condition expressed in Eq. (11). These equations reveal, for any combination of C_{p_b} and F, the velocity V_S remains finite on the cavity boundary. This suggests that there does not exist a stagnation point on the cavity-fluid interface, implying that the cavity either extends to infinity, or streamlines, comprising the cavity boundary, turn back and form a reentrant jet. Experimental evidence suggests that the latter is the case. Because all the streamlines cannot turn back, there must exist a stagnation point in the fluid medium on the body-cavity axis very near the rear end of the cavity. From this point of view, one may choose a rear stagnation point, and abandon the enforcement of constant pressure condition in its vicinity by prescribing the decay of tangential velocity V_S in some arbitrary fashion from a chosen point (maximum radius) on the cavity. As discussed below, the numerical experiments made in such a manner have become very complex, and are not too successful since the solution has not converged at the rear end of the cavity. But, it has revealed that the solution on the front end of the cavity, especially in the neighborhood of the body base, is quite insensitive to the inaccuracy of the solution at the rear end. In engineering applications, the major interest lies in the solution on the body rather than in the details of the cavity. For this reason, all the numerical results obtained to date are achieved by applying the constant pressure condition on the front portion of the cavity alone.

It may be pointed out here, that Chou[2] employs a rear stagnation point model, and replaces the pressure condition with a prescribed cavity configuration (CONE) near the stagnation point.

Numerical Computations

In the analytical formulation, the integrals extend over the entire cavity length, L_c, which is unknown. To start the computations, the cavity configuration is approximated as a cylindrical extension of the body, with a spherical cap at its end. Furthermore, the length of the cavity is arbitrarily set equal to one body length. In the earlier computations, attempts were made to enforce the constant pressure condition on the straight portion, and an arbitrarily chosen decay of tangential velocity on the spherical portion, of the cavity. The cavity length, as well as its shape, were updated before a new iteration was begun, but the functional form of the tangential velocity decay on the rear end of the cavity was kept unchanged. If the solution had converged, this procedure would have yielded the appropriate cavity length and the configuration as a function of Froude and cavitation numbers. Unfortunately, the results indicated that a good starting cavity configuration, as well as a more realistic description of velocity decay in the neighborhood of the rear stagnation point, are required to obtain convergence of solution. The cavity configuration and velocity decay obtained from slender body theory (Ref. 2) would probably form a good starting solution, but this needed additional computational effort. In addition, modifications to the already complicated computer code were required to accommodate the increase or decrease of nodal points as the cavity length changed during each iteration. Due to expediency, further numerical trials, to evaluate more fully the cavity configurations, were dropped in favor of enforcing constant-pressure condition on the forward portion of the cavity surface, ignoring the rearward part of the cavity. Such a solution obviously is approximate, but was felt satisfactory for the purpose of evaluating the influence of the cavity on the pressure distribution of the body.

This simplification eliminates the need for prior knowledge of cavity length, L_c. In the numerical computations reported here, the portion of the cavity on which constant-pressure condition was enforced is equal to about one-half of the body length, irrespective of the Froude and cavitation numbers used. For the range of those parameters of practical interest, the cavity length is equal to about one body length, and the maximum cavity radius occurs at less than three-quarters of its length from the base. Thus, for these cases, the constant-pressure condition is enforced over the cavity almost up to the maximum-radius position beyond which the tangential velocity is expected to decay. For large Froude numbers, the maximum-radius position shifts further away from the base, and may require the constant-pressure condition to be enforced over a larger distance than in the present computations.

III. Results

In an effort to validate the computational technique presented here, some comparisons of the computed results with measurements are made in this section. Comparisons with precise wind tunnel pressure data obtained under steady-state flow conditions are made, as well as with data obtained from free-flight, quasisteady underwater launch tests. Figure 2 presents the present solution method pressure distribution for an axisymmetric body with a blunt base. The corresponding experimental data were obtained in a low-speed wind tunnel with pressure transducers located all along the horizontally mounted body. In the analytical simulation, the measured base pressure coefficient, $C_{p_b} = -0.169$, was the cavity pressure input, and gravitational effects were ignored by assigning the Froude number a very large value. The agreement between theory and experiment is extremely good.

The comparison of the predicted and measured pressure distribution of a free-flight body of revolution launched vertically underwater is shown in Fig. 3. These experimental results represent a quasisteady average of five sets of data measured during a vertically ascending trajectory. This experimental case represented a flow condition of zero angle of attack, a base pressure coefficient of 0.172 and a Froude number $= (3.88)^{1/2}$. The pressures near the base were measured on both the $\theta = 0$ deg, as well as the $\theta = 180$ deg side of the body. The agreement between theory and experiment is quite good, in general, over most of the body.

The computed cavity configuration is also compared with the test data in Fig. 3. The shaded area represents the range of photographic data depicting the external bounds of the cavity. The cavity size is greatly influenced by the base pressure coefficient, C_{p_b}. The larger this coefficient, the larger the radius of the cavity. The typical variation of cavity size with base pressure is evident from the photographs shown in Fig. 4.

The comparisons of simulated and measured pressure data near the base of a body of revolution launched vertically, is shown for various flight conditions in Fig. 5. Note that the analytical simulation corresponds to a steady-state condition, while the experimental data has some transient effects since the body velocity is still changing, although slightly, at the instant the data was chosen for comparison. In view of this, the agreement seems to be reasonable in the range of Froude numbers and base pressure coefficients tested here.

Two significant inferences that can be drawn from this comparison are: 1) the pressure decay on the missile near the base is not strongly dependent on the Froude number; and 2) the effect of the cavity extends farther from the base, the larger the base pressure. Such a result suggests that the cavity shape in the vicinity of the base is more sensitive to the cavity pressure than it is to Froude number. Figure 6 presents the sensitivity of the cavity shape in the vicinity of the body on the base pressure coefficient, C_{p_b}. Note that for positive coefficients the cavity expands, and its radius is larger than the base radius, while the converse is true for negative coefficients. When $C_{p_b} = 0$, the flow along the cavity boundary still expands to cancel the increase in hydrostatic pressure and to reduce the streamline to a constant pressure line. This is why the radius of the cavity is larger than the base radius in Fig. 6 for $C_{p_b} = 0$. Note that as the Froude number increases, or the effect of gravity field reduces, the cavity tends to be straight for this pressure condition, and becomes a straight cylinder when $F \to \infty$, or the gravity term is omitted in the pressure equation.

Finally, the present analysis is compared to the earlier analyses of the body-cavity flow problem in which singularities are located along the axis of symmetry and the slender body assumption is invoked. For the purpose of comparison, a 5 deg cone was chosen. The pressure distributions on the cone and cavity configuration in the vicinity of the base are

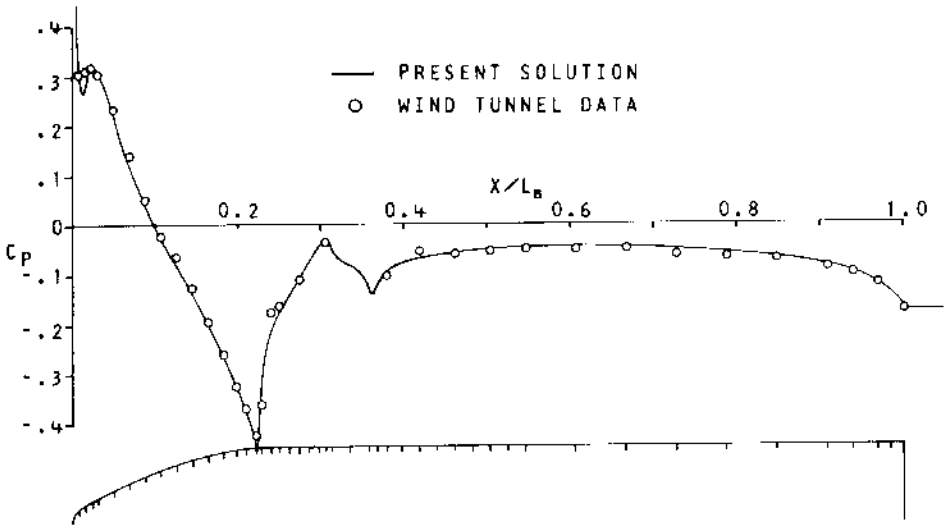

Fig. 2 Pressure distribution on a blunt-based axisymmetric body ($C_{p_b} = -0.169$, $F^2 = \infty$).

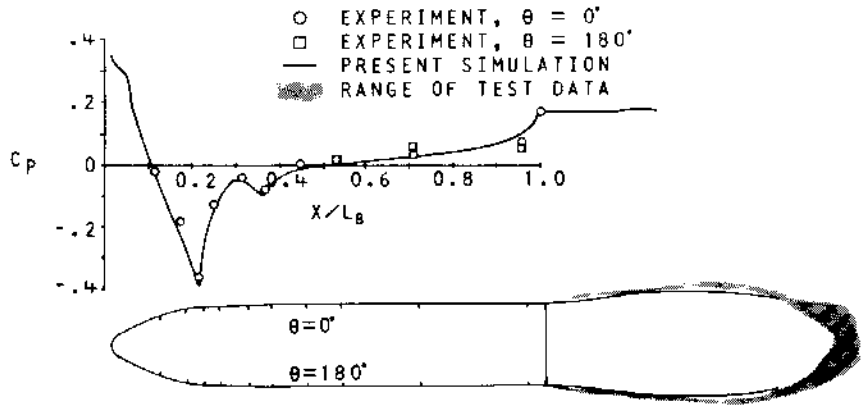

Fig. 3 Pressure distribution and cavity configuration in vertical free-flight ($\alpha = 0$ deg, $C_{p_b} = 0.172$, $F^2 = 3.88$).

compared in Figs. 7 and 8, respectively. The Froude and cavitation numbers (negative pressure coefficient) at which this comparison is made are within the limits of slender body assumption, and the pressure distributions, as expected, agree quite well. However, they are not exactly identical, as is evident from the comparison made in Fig. 7 where the pressure scale is purposefully magnified. In the range of higher cavitation and lower Froude numbers of practical interest, the difference in pressure predictions between slender body theory and the present solution would be larger than shown here. Experience has shown that even the pressure differences of this small a magnitude contribute significantly to certain hydrodynamic coefficients of blunt-based bodies. For this reason, it is recommended that for accurate predictions of hydrodynamic performance, especially stability of bodies of revolution, the Neumann solution should be used instead of slender body theory.

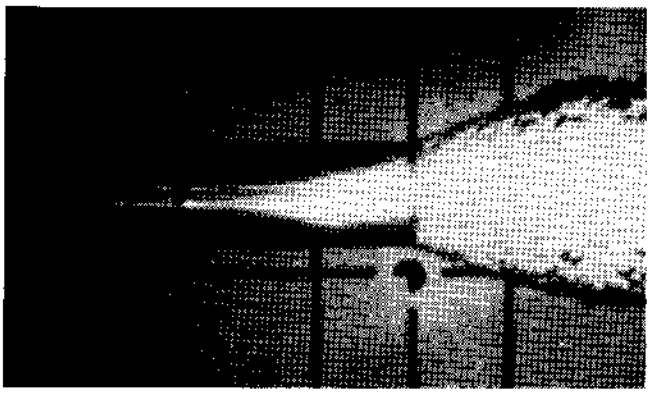

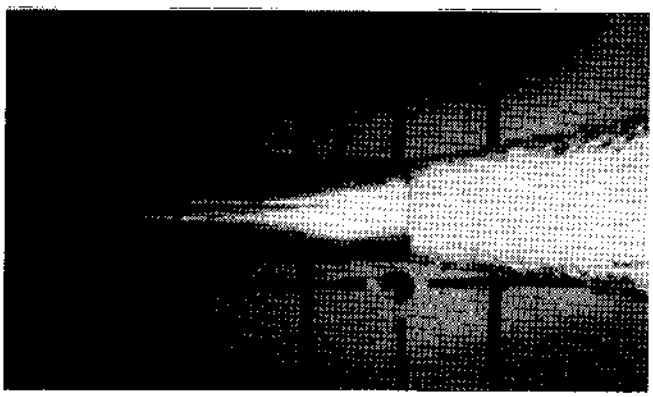

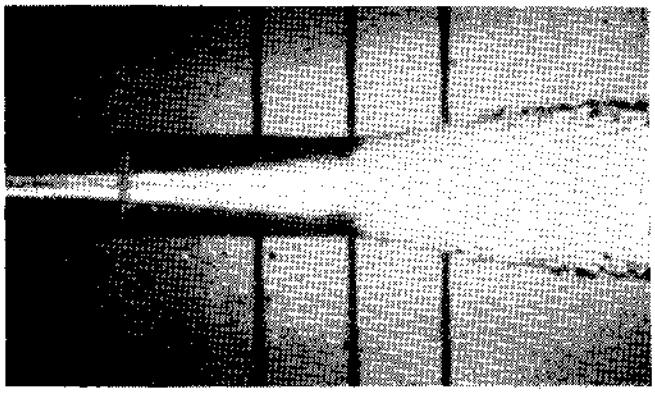

Fig. 4 Typical cavity boundaries behind blunt axisymmetric bodies at high C_{p_b} (top), medium C_{p_b} (center), and low C_{p_b} (bottom).

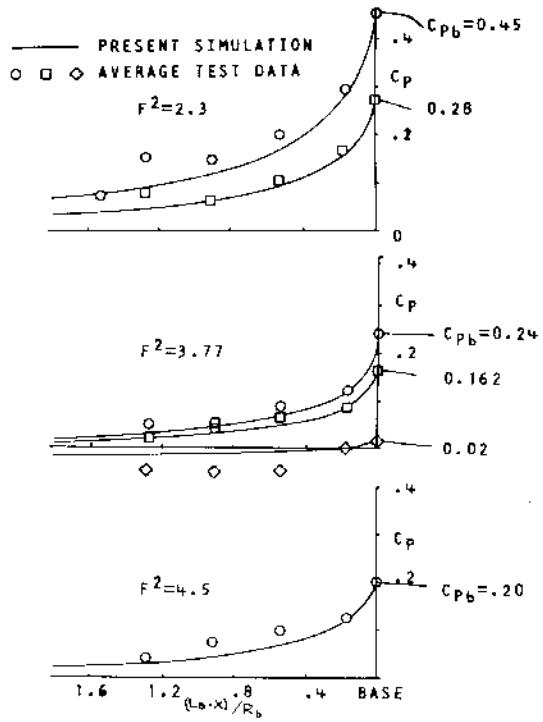

Fig. 5 Comparison of simulated and measured pressures in free-flight near base of axisymmetric body.

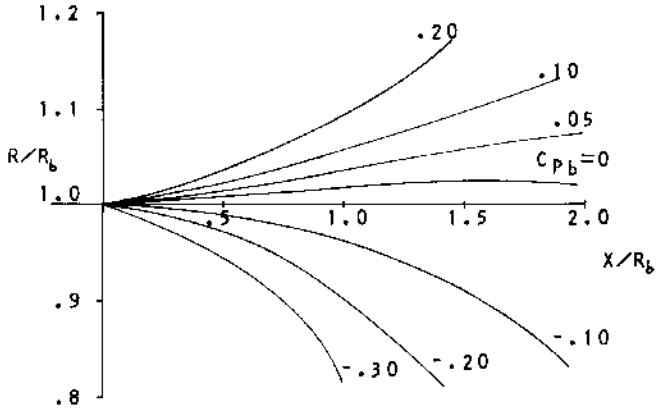

Fig. 6 Cavity shape in the vicinity of the base as effected by the base pressure ($F^2 = 4.0$).

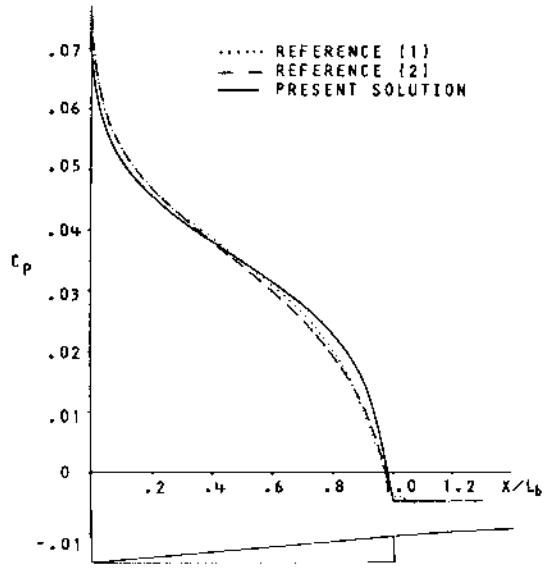

Fig. 7 Pressure distribution for a 5 deg cone at $C_{p_b} = -0.0042$ and $F^2 = \infty$.

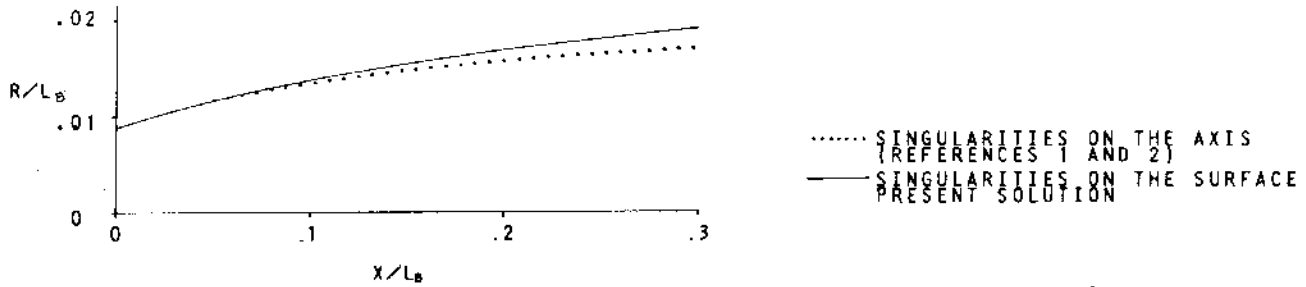

Fig. 8 Cavity boundary configuration for a 5 deg cone in the vicinity of its base ($C_{p_b} = -0.0042$, $F^2 - \infty$).

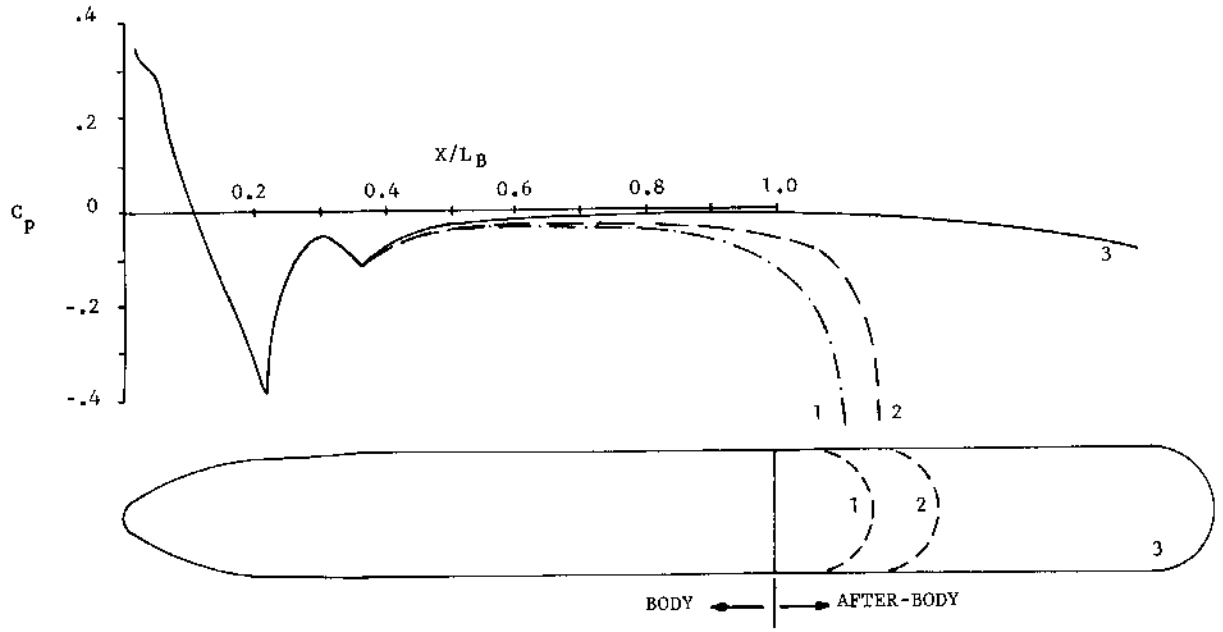

Fig. 9 Pressure distribution for different after-body lengths.

To this point, the potential flow problem with mixed boundary conditions has been avoided simply by approximating the cavity as a rigid cylindrical extension of the missile by a finite length with a hemispherical cap at the end (see Fig. 9). The pressure distributions on the missile obtained for different extension lengths are shown in Fig. 9. The pressure coefficient near the base is always negative and the pressure curves, as would be expected, look like those that could be obtained for negative values of C_{p_b}. The shorter the length of the extension, the more negative is the value of the C_{p_b} for the pressure curve. Thus, the approximate method may possibly yield somewhat realistic results for the range of C_{p_b} less than zero, but not for positive values of C_{p_b}.

IV. Conclusions

In the past, the flows past bodies of revolution with blunt bases launched vertically have been analyzed, using one or more of the following assumptions: 1) the body is slender; 2) the gravitation effect is negligible; and 3) the cavity trailing the body can be treated as an extension of the rigid body itself. The present analysis makes no such assumptions, and obtains the solution by an iterative technique that satisfies the appropriate boundary conditions both on the body and on the trailing cavity in the vicinity of the base. The effects of the tail end of the cavity on the body and the fore-cavity, though they should be included, are shown to be not critical. This inference was drawn from the comparisons made between the computed results and the measured data over a range of Froude numbers, and base pressure coefficients of practical interest. The computed effects of the trailing cavity on the body are shown to be consistent with actual measurements in free-flight simulations.

The comparison of pressure distribution on a body of revolution has indicated that Neumann solution matches exactly with measurements. Using this as a criterion, it was inferred that slender body theory provides slightly different results even within its range of applicability.

Acknowledgments

This work was supported in part by Missile Systems Division of Lockheed Missiles & Space Company, Inc., under its Independent Development Program.

References

[1] Cuthbert, J. and Street, R., "An Approximate Theory for Supercavitating Flow About Slender Bodies of Revolution," Lockheed Missiles and Space Co., Inc., Sunnyvale, Calif., TM 81-73-39, Sept. 1964.

[2] Chou, Y.S., "Axisymmetric Cavity Flows Past Slender Bodies of Revolution," *Journal of Hydronautics,* Vol. 8, No. 1, Jan. 1974, pp. 13-18.

[3] Struck, H.G., "Discontinuous Flows and Free Streamline Solutions for Axisymmetric Bodies at Zero and Small Angle of Attack," NASA TND-5634, Feb. 1970.

[4] Smith, A.M.O. and Pierce, J., "Exact Solution of the Neumann Problem, Calculation of Noncirculatory Plane and Axially Symmetric Flows About or Within Arbitrary Boundaries," Douglas Report No. ES 26988, April 25, 1958.

[5] Johnstone, R.S., "A Mathematical Model for a Three Degree of Freedom Simulation of the Underwater Launch of a Rigid Missile," Lockheed Missiles & Space Co., Inc., Sunnyvale, Calif., TM 5774-69-21, May 1969.

[6] Rattayya, J.V. and Chisholm, M.A., "Calculation of Hydrodynamic Coefficients Using the Modified Douglas-Neumann Computer Program," Lockheed Missiles & Space Co., Inc., Sunnyvale, Calif., TM 5724-75-38, April 1975.